

Article

Design and Implementation of the Battery Energy Storage System in DC Micro-Grid Systems

Yuan-Chih Chang *, Hao-Chin Chang and Chien-Yu Huang

Department of Electrical Engineering and Advanced Institute of Manufacturing with High-Tech Innovations, National Chung Cheng University, Chiayi 62102, Taiwan; aloner330@gmail.com (H.-C.C.); apr3693@gmail.com (C.-Y.H.)

* Correspondence: ycchang@ccu.edu.tw; Tel.: +886-5-272-9108

Received: 25 May 2018; Accepted: 12 June 2018; Published: 14 June 2018



Abstract: The design and implementation of the battery energy storage system in DC micro-grid systems is demonstrated in this paper. The battery energy storage system (BESS) is an important part of a DC micro-grid because renewable energy generation sources are fluctuating. The BESS can provide energy while the renewable energy is absent in the DC micro-grid. The circuit topology of the proposed BESS will be introduced. The design of the voltage controller and the current controller for the battery charger/discharger are also illustrated. Finally, experimental results are provided to validate the performance of the BESS.

Keywords: battery energy storage system; DC micro-grid; voltage control; current control

1. Introduction

Reducing carbon emissions and mitigating the global warming are the main advantages of using renewable energy [1–3]. However, renewable energy fluctuates with its environmental parameters. Therefore, an AC microgrid [4–6] and a DC microgrid [7–9] are implemented to treat this issue. Renewable energy in a microgrid can be solar or wind power. Extra electricity can be stored in an energy storage system [10–13]. If the renewable energy sources are absent, the micro-grid will be stabilized via the energy storage system. In this paper, the battery energy storage system (BESS) is designed and implemented in a DC micro-grid.

Takagi-Sugeno Fuzzy [14], proposed by Takagi and Sugeno, is a control system based on fuzzy-logic. In T-S Fuzzy systems, a nonlinear system can be resembled by linear sub-systems. The controllers of the T-S Fuzzy system are designed on the concept of parallel-distributed compensation (PDC) [15]. Lyapunov theorem [16] can be applied to prove the stability of a T-S Fuzzy control system. The stability specifications are displayed in the form of linear matrix inequality (LMI). The T-S Fuzzy control applied to the DC-DC converter can be classified as buck [17] and boost [18] converters. Nevertheless, the non-ideal characteristics of the circuit elements are not treated in the literature. The non-ideal circuit elements are treated in this research to increase control precision and performance.

A battery energy storage system in DC micro-grid systems is designed and implemented. A BESS consists of the battery and the charger/discharger. A buck converter, combined with a boost converter, is implemented as the charger/discharger. If the battery needs to be charged, the buck converter is operated as a charger. Furthermore, the boost converter is operated as a discharger to release electric energy. In this paper, the BESS in the DC micro-grid system is first illustrated. Next, the circuit topology, considering non-ideal circuit models, is demonstrated. After that, the state equations of the BESS are obtained through the state-space average scheme. Then, the voltage and current controllers of the BESS are designed via T-S Fuzzy controls. The system stability of the BESS is proved and

verified. The control performances of the voltage controller and current controller are validated by experimental results.

2. System Configuration

The system configuration of the DC micro-grid is shown in Figure 1. The developed battery energy storage system consists of the battery and the bidirectional DC/DC converter. Figure 2 shows the circuit configuration of the battery charger/discharger. The buck converter and boost converter is combined to form the bidirectional converter. In charging mode, the buck converter is operated with (M_1, D_2) , while in discharging mode, the boost converter is operated with (M_2, D_1) . The non-ideal circuit elements are included in the circuit configuration. The non-ideal elements include the equivalent series resistance (ESR) of the power switch (R_M), the ESR of the inductor (R_L), the ESR of the capacitor ($R_{C_B}, R_{C_{DC}}$), and the forward conduction voltage of the diode (V_D). Inductance current i_L , DC-link voltage V_{DC} and battery voltage V_B are used to determine the duty ratio of the power switches. The feedback signals are sampled by the analog-to-digital converter (ADC). The control of the bidirectional DC/DC converter is digitally realized via the microcontroller Renesas RX62T.

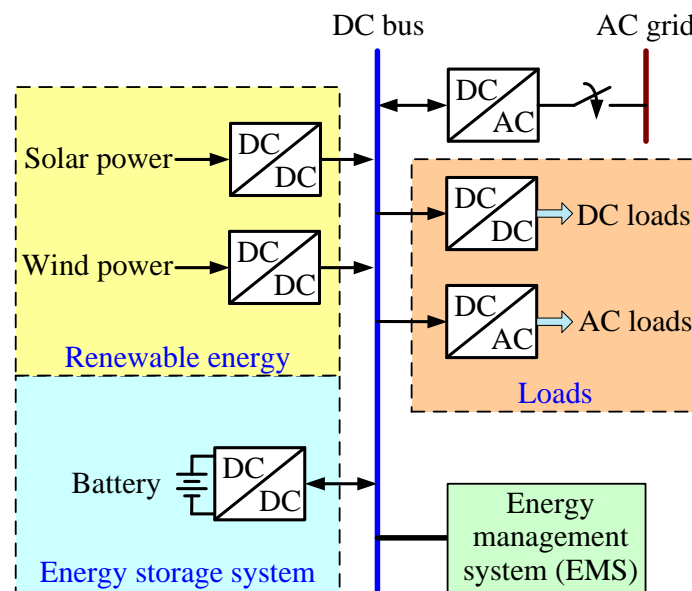


Figure 1. System configuration of the DC micro-grid.

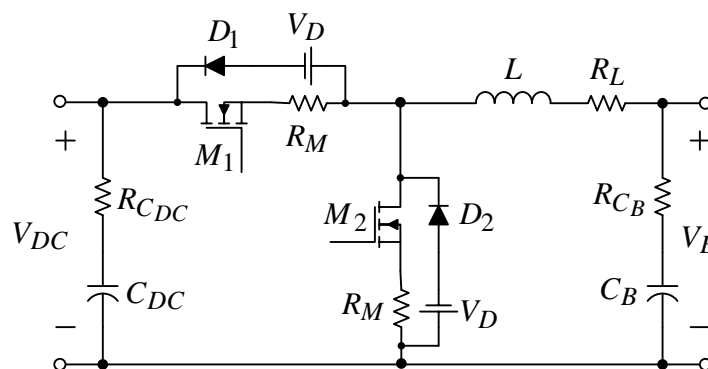


Figure 2. Circuit configuration of the battery charger/discharger.

3. Operation Modes and State Equations

3.1. Charging Mode

At charging mode, the power switch M_2 is kept off. The duty ratio of the power switch M_1 is controlled to regulate the inductance current. When M_1 is turned on, the inductance will be magnetized and the inductance current rises. When M_1 is turned off, the diode D_2 will be forced to turn on. Then the inductance is de-magnetized and the inductance current will fall.

The state space average scheme can be used to find the state equations of charging mode:

$$\begin{bmatrix} \dot{i}_L \\ \dot{V}_{C_B} \end{bmatrix} = \begin{bmatrix} -\frac{1}{L} \left(R_L + \frac{RR_{C_B}}{R+R_{C_B}} \right) & -\frac{R}{L(R+R_{C_B})} \\ \frac{R}{C_B(R+R_{C_B})} & -\frac{1}{C_B(R+R_{C_B})} \end{bmatrix} \begin{bmatrix} i_L \\ V_{C_B} \end{bmatrix} + \begin{bmatrix} \frac{1}{L}(V_{DC} + V_D - i_L R_M) \\ 0 \end{bmatrix} D + \begin{bmatrix} -\frac{V_D}{L} \\ 0 \end{bmatrix} \quad (1)$$

where R is the load resistance and D is the duty ratio of M_1 . The output is the inductance current:

$$y = i_L = \begin{bmatrix} 1 & 0 \end{bmatrix} \begin{bmatrix} i_L \\ V_{C_B} \end{bmatrix} \quad (2)$$

3.2. Discharging Mode

At discharging mode, the power switch M_1 is kept off. The duty ratio of the power switch M_2 is controlled to regulate the output voltage. When M_2 is turned on, the inductance current rises. When M_2 is turned off, the diode D_1 will be forced to turn on. Then, the inductance current falls.

The state space average scheme is also used to find the state equations of discharging mode:

$$\begin{bmatrix} \dot{i}_L \\ \dot{V}_{C_{DC}} \end{bmatrix} = \begin{bmatrix} -\frac{1}{L} \left(R_L + \frac{RR_{C_{DC}}}{R+R_{C_{DC}}} \right) & -\frac{R}{L(R+R_{C_{DC}})} \\ \frac{R}{C_{DC}(R+R_{C_{DC}})} & -\frac{1}{C_{DC}(R+R_{C_{DC}})} \end{bmatrix} \begin{bmatrix} i_L \\ V_{C_{DC}} \end{bmatrix} + \begin{bmatrix} \frac{1}{L} \left[V_D + \left(\frac{RR_{C_{DC}}}{R+R_{C_{DC}}} - R_M \right) i_L + \frac{R}{R+R_{C_{DC}}} V_{C_{DC}} \right] \\ -\frac{1}{C_{DC}(R+R_{C_{DC}})} i_L \end{bmatrix} D + \begin{bmatrix} \frac{V_B - V_D}{L} \\ 0 \end{bmatrix} \quad (3)$$

where D is the duty ratio of M_1 . The output is the DC-link voltage:

$$y = V_{DC} = \begin{bmatrix} \frac{RR_{C_{DC}}}{R+R_{C_{DC}}} & \frac{R}{R+R_{C_{DC}}} \end{bmatrix} \begin{bmatrix} i_L \\ V_{C_{DC}} \end{bmatrix} - \frac{RR_{C_{DC}}}{R+R_{C_{DC}}} i_L D \quad (4)$$

4. Design of Current Controller and Voltage Controller

In charging/discharging mode, the current/voltage tracking error will converge to zero by defining a new state variable:

$$x_{err}(t) = \int (r - y(t)) dt \quad (5)$$

where r is desired value of inductance current for charger and output voltage for discharger.

By combining Equations (1), (2) and (5), the expanded state equations of the charger can be obtained as:

$$\begin{bmatrix} \dot{i}_L \\ \dot{V}_{C_B} \\ \dot{x}_{err} \end{bmatrix} = \begin{bmatrix} -\frac{1}{L} \left(R_L + \frac{RR_{C_B}}{R+R_{C_B}} \right) & -\frac{R}{L(R+R_{C_B})} & 0 \\ \frac{R}{C_B(R+R_{C_B})} & -\frac{1}{C_B(R+R_{C_B})} & 0 \\ -\frac{RR_{C_B}}{R+R_{C_B}} & -\frac{R}{R+R_{C_B}} & 0 \end{bmatrix} \begin{bmatrix} i_L \\ V_{C_B} \\ x_{err} \end{bmatrix} + \begin{bmatrix} \frac{1}{L}(V_{DC} + V_D - i_L R_M) \\ 0 \\ 0 \end{bmatrix} D + \begin{bmatrix} -\frac{V_D}{L} \\ 0 \\ r \end{bmatrix} \quad (6)$$

$$y = \begin{bmatrix} 1 & 0 & 0 \end{bmatrix} \begin{bmatrix} i_L \\ V_{C_{DC}} \\ x_{err} \end{bmatrix} \tag{7}$$

Furthermore, by combining Equations (3)–(5), the expanded state equations of the discharger can be obtained as:

$$\begin{bmatrix} \dot{i}_L \\ \dot{V}_{C_{DC}} \\ \dot{x}_{err} \end{bmatrix} = \begin{bmatrix} -\frac{1}{L} \left(R_L + \frac{RR_{C_{DC}}}{R+R_{C_{DC}}} \right) & -\frac{R}{L(R+R_{C_{DC}})} & 0 \\ \frac{R}{C_{DC}(R+R_{C_{DC}})} & -\frac{1}{C_{DC}(R+R_{C_{DC}})} & 0 \\ -\frac{RR_{C_{DC}}}{R+R_{C_{DC}}} & -\frac{R}{R+R_{C_{DC}}} & 0 \end{bmatrix} \begin{bmatrix} i_L \\ V_{C_{DC}} \\ x_{err} \end{bmatrix} \tag{8}$$

$$+ \begin{bmatrix} \frac{1}{L} \left[V_D + \left(\frac{RR_{C_{DC}}}{R+R_{C_{DC}}} - R_M \right) i_L + \frac{R}{R+R_{C_{DC}}} V_{C_{DC}} \right] \\ -\frac{1}{C_{DC}(R+R_{C_{DC}})} i_L \\ \frac{RR_{C_{DC}}}{R+R_{C_{DC}}} i_L \end{bmatrix} D + \begin{bmatrix} \frac{V_B - V_D}{L} \\ 0 \\ r \end{bmatrix}$$

$$y = V_{DC} = \begin{bmatrix} \frac{RR_{C_{DC}}}{R+R_{C_{DC}}} & \frac{R}{R+R_{C_{DC}}} & 0 \end{bmatrix} \begin{bmatrix} i_L \\ V_{C_{DC}} \\ x_{err} \end{bmatrix} - \frac{RR_{C_{DC}}}{R+R_{C_{DC}}} i_L D \tag{9}$$

For convenience, Equations (6) and (8) are represented in general state-equation form:

$$\dot{x}(t) = Ax(t) + Bu(t) + Ev(t) \tag{10}$$

where $v(t)$ are the disturbances of the system.

In the T-S fuzzy models, the nonlinear BESS are represented by linear sub-systems according to the model rules:

Model rules i : If $z_1(t)$ is M_{i1} and ... and $z_p(t)$ is M_{ip} , then

$$\dot{x}(t) = A_i x(t) + B_i u(t) \tag{11}$$

where $u(t)$ are the control inputs, $x(t)$ are the state variables, A_i, B_i are the state matrices of the sub-systems, M_{ip} is the fuzzy set. In charging mode, i_L is chosen as $z_p(t)$. In discharging mode, $i_L, V_{C_{DC}}$ are chosen as $z_p(t)$. The T-S fuzzy system of the BESS can be expressed after defuzzification:

$$\dot{x}(t) = \sum_{i=1}^r h_i(z(t)) \{ A_i x(t) + B_i u(t) \} \tag{12}$$

where:

$$h_i(z(t)) = \frac{\prod_{j=1}^r M_{ij}(z_j(t))}{\sum_{i=1}^r \prod_{j=1}^r M_{ij}(z_j(t))} \tag{13}$$

and $M_{ij}(z_j(t))$ is the grad of membership.

The PDC controllers of the BESS are expressed as:

Control rules i : If $Z_1(t)$ is M_{i1} and ... and $z_p(t)$ is M_{ip} , then

$$u(t) = -\sum_{i=1}^r h_i(z(t)) F_i x(t) \tag{14}$$

By substituting (14) into (12), the close-loop system are obtained:

$$\dot{x}(t) = \sum_{i=1}^r \sum_{j=1}^r h_i(z(t)) h_j(z(t)) \{ A_i - B_i F_j \} x(t) \tag{15}$$

According to state Equation (10), the BESS T-S fuzzy system with disturbances is found:

$$\begin{aligned} \dot{x}(t) &= \sum_{i=1}^r h_i(z(t)) \{A_i x(t) + B_i u(t) + E_i v(t)\} \\ y(t) &= \sum_{i=1}^r h_i(z(t)) C_i x(t) \end{aligned} \quad (16)$$

To suppress the disturbances, the H_∞ performance index is defined:

$$\sup_{\|v(t)\|_2 \neq 0} \frac{\|y(t)\|_2}{\|v(t)\|_2} \leq \gamma, \quad 0 \leq \gamma \leq 1 \quad (17)$$

where γ is the disturbance suppression ability index.

To analyze the stability of the designed current and voltage controller, Lyapunov theorem [19] is applied to find the following LMI condition:

$$\begin{bmatrix} XA_i^T - M_j^T B_i^T + A_i X - B_i M_j & E_i & -XC_i^T \\ E_i^T & -\gamma^2 I & 0 \\ -C_j X & 0 & -I \end{bmatrix} < 0, \quad i \leq j \quad (18)$$

where X is a positive definite matrix and $X = P^{-1}$, $M_j = F_j X$.

5. Results and Discussions

Table 1 lists the specifications of the BESS.

For buck mode, the H_∞ performance index is selected as $\gamma = 0.7$. For boost mode, the H_∞ performance index is selected as $\gamma = 0.8$. The controller gains F_i are obtained by using the LMI toolbox in MATLAB.

Table 1. Specifications of the BESS.

Rated power	2 kW	V_D	1.5 V
Inductance	1.97 mH	R_M	0.079 $\dot{\text{U}}$
Input voltage	380 V (DC)	Input capacitance	560 μF
Output voltage	100 V (DC)	Output capacitance	440 μF

5.1. Charging Mode

The load resistance is constant and the input voltage V_{DC} is 380 V. The current commands are 5 A and 20 A. The inductance current and battery voltage at current command 5 A, load = 20 $\dot{\text{U}}$ (500 W), and current command 20 A, load = 5 $\dot{\text{U}}$ (2 kW) are shown in Figure 3a,b, respectively. It can be found that the inductance current can accurately track the command.

Next, the load is constant (10 $\dot{\text{U}}$) and the input voltage V_{DC} is also 380 V. The current command is variable 5 A \rightarrow 10 A \rightarrow 5 A. Figure 4 shows the inductance current and battery voltage with current command variation. It is clear that the inductance current tracks the command accurately.

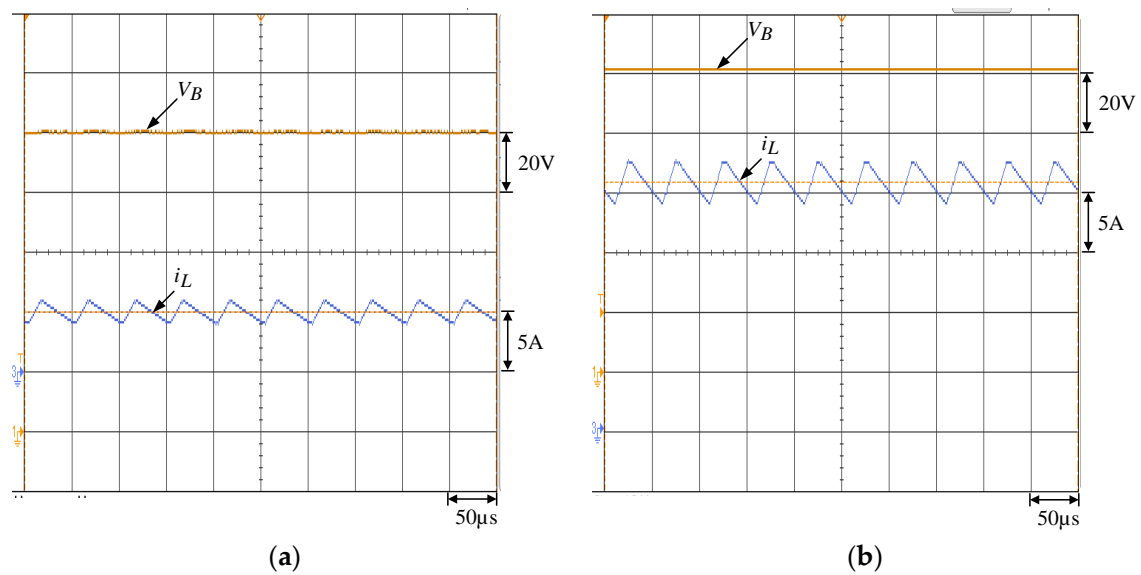


Figure 3. Inductance current and battery voltage at constant load resistance: (a) current command 5 A, 20 V (500 W); (b) current command 20 A, 5 V (2 kW).

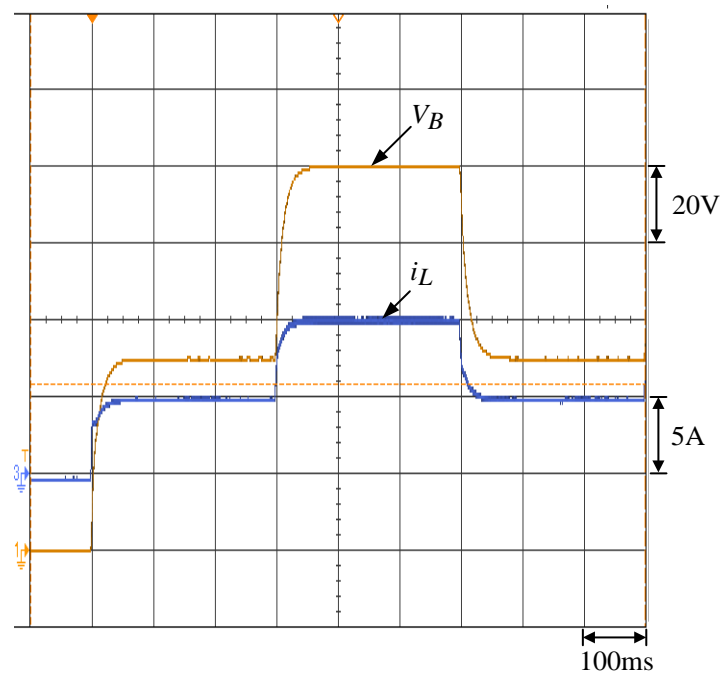


Figure 4. Inductance current and battery voltage with current command variation 5 A → 10 A → 5 A (load 10 V).

5.2. Discharging Mode

The load resistance is constant and the input battery voltage V_B is 100 V. Figure 5a,b shows the inductance current and DC-link voltage at load = 250 W (577.6 W) and 135.7 W (1.06 kW), respectively. It is obvious that the DC-link voltage can exactly track the command 380 V.

Next, the input voltage V_B is 90 V, and the load is variable 250 W → 135.7 W → 250 W. Figure 6a,b shows the inductance current and DC-link voltage under load variation 300 W → 150 W and 150 W → 300 W. It can be seen that the DC-link voltage is well regulated under load variation.

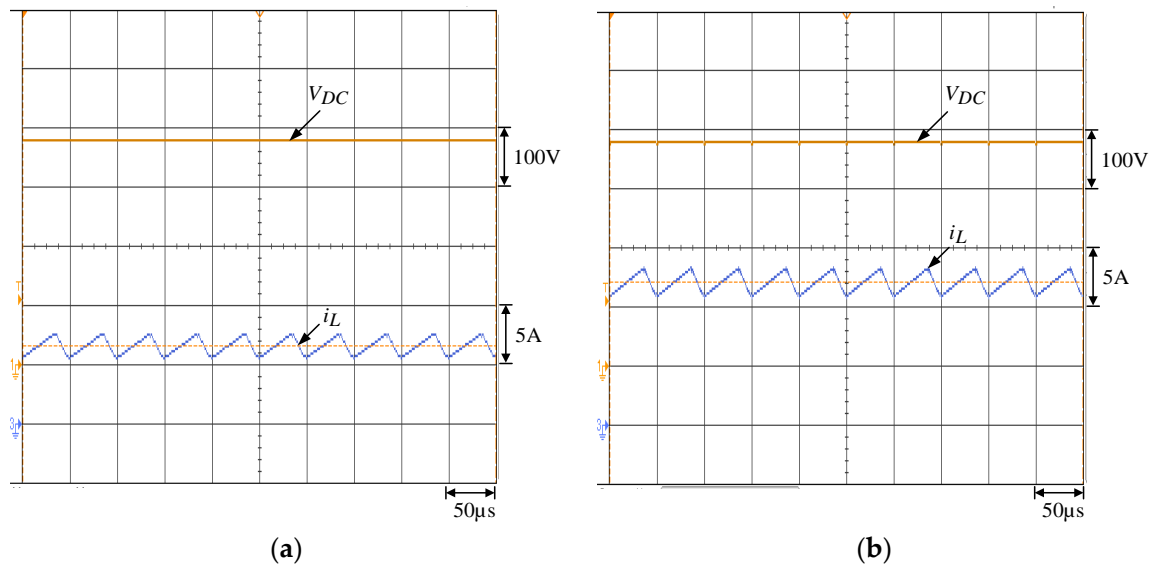


Figure 5. Inductance current and DC-link voltage at constant load: (a) 250 \hat{U} (577.6 W); (b) 135.7 \hat{U} (1.06 kW).

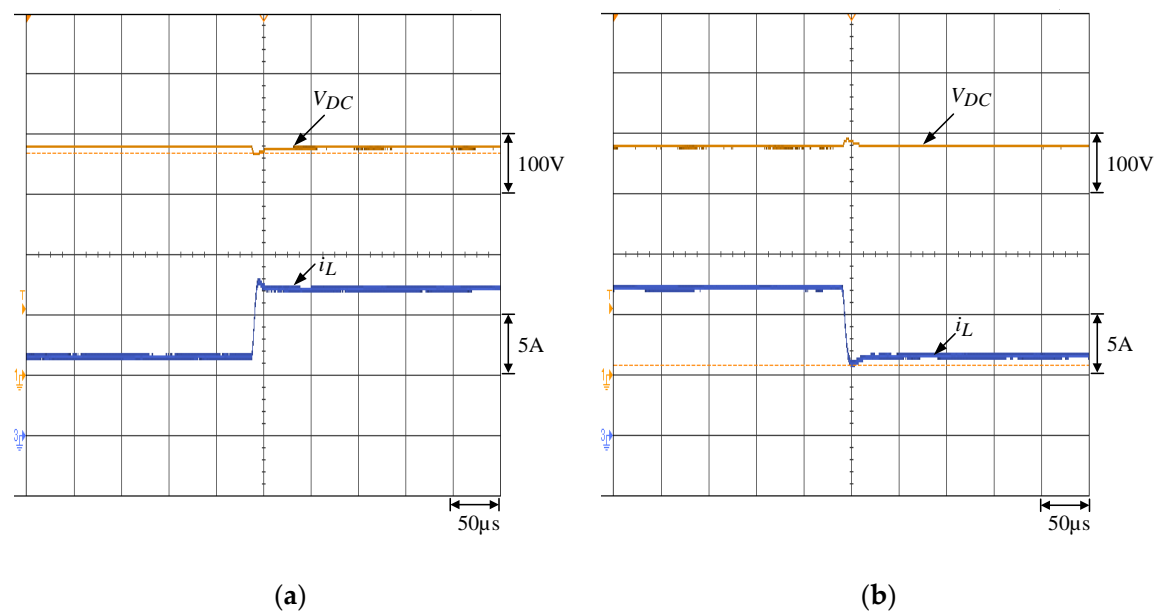


Figure 6. Inductance current and DC-link voltage under load variation: (a) 250 $\hat{U} \rightarrow 135.7 \hat{U}$; (b) 135.7 $\hat{U} \rightarrow 250 \hat{U}$.

6. Conclusions

A battery energy storage system in DC micro-grid systems is designed and implemented. T-S Fuzzy current control and voltage control of the BESS is introduced. The system stability with disturbance suppression ability is analyzed and shown. The performance of the current controller and voltage controller is verified via experimental results.

Author Contributions: The authors contributed equally to this work.

Funding: This research was supported by the Ministry of Science and Technology, Taiwan, under the Grant of MOST 106-2221-E-194-037.

Conflicts of Interest: The authors declare no conflict of interest.

References

1. Carrizosa, M.J.; Arzandé, A.; Navas, F.D.; Damm, G.; Vannier, J.-C. A control strategy for multiterminal DC grids with renewable production and storage devices. *IEEE Trans. Sustain. Energy* **2018**, *9*, 930–939. [[CrossRef](#)]
2. Dahmani, O.; Bourguet, S.; Machmoum, M.; Guerin, P.; Rhein, P.; Josse, L. Optimization and reliability evaluation of an offshore wind farm architecture. *IEEE Trans. Sustain. Energy* **2017**, *8*, 542–550. [[CrossRef](#)]
3. Sharma, S.K.; Chandra, A.; Saad, M.; Lefebvre, S.; Asber, D.; Lenoir, L. Voltage flicker mitigation smart loads with high penetration of renewable energy in distribution systems. *IEEE Trans. Sustain. Energy* **2017**, *8*, 414–424. [[CrossRef](#)]
4. Sahoo, S.K.; Sinha, A.K.; Kishore, N.K. Control techniques in AC, DC, and hybrid AC-DC microgrid: A review. *IEEE J. Emerg. Sel. Top. Power Electron.* **2018**, *6*, 738–759. [[CrossRef](#)]
5. Kim, J.; Guerrero, J.M.; Rodriguez, P.; Teodorescu, R.; Nam, K. Mode adaptive droop control with virtual output impedances for an inverter-based flexible AC microgrid. *IEEE Trans. Power Electron.* **2011**, *26*, 689–701. [[CrossRef](#)]
6. Han, R.; Meng, L.; Ferrari-Trecate, G.; Coelho, E.A.A.; Vasquez, J.C.; Guerrero, J.M. Containment and consensus-based distributed coordination control to achieve bounded voltage and precise reactive power sharing in islanded AC microgrids. *IEEE Trans. Ind. Appl.* **2017**, *53*, 5187–5199. [[CrossRef](#)]
7. Wang, M.-H.; Mok, K.-T.; Tan, S.-C.; Hui, S.Y. Multifunctional DC electric springs for improving voltage quality of DC grids. *IEEE Trans. Smart Grid* **2018**, *9*, 2248–2258. [[CrossRef](#)]
8. Kumar, M.; Srivastava, S.C.; Singh, S.N. Control strategies of a DC microgrid for grid connected and islanded operations. *IEEE Trans. Smart Grid* **2015**, *6*, 1558–1601. [[CrossRef](#)]
9. Radwan, A.A.A.; Mohamed, Y.A.-R.I. Linear active stabilization of converter-dominated DC microgrids. *IEEE Trans. Smart Grid* **2012**, *3*, 203–216. [[CrossRef](#)]
10. Abeywardana, D.B.W.; Hredzak, B.; Agelidis, V.G. A fixed-frequency sliding mode controller for a boost-inverter-based battery-supercapacitor hybrid energy storage system. *IEEE Trans. Power Electron.* **2017**, *32*, 668–680. [[CrossRef](#)]
11. Ciccirelli, F.; Iannuzzi, D.; Kondo, K.; Fratelli, L. Line-voltage control based on wayside energy storage systems for tramway networks. *IEEE Trans. Power Electron.* **2016**, *31*, 884–899. [[CrossRef](#)]
12. Akter, M.P.; Mekhilef, S.; Tan, N.M.L.; Akagi, H. Modified model predictive control of a bidirectional AC-DC converter based on Lyapunov function for energy storage systems. *IEEE Trans. Ind. Electron.* **2016**, *63*, 704–715. [[CrossRef](#)]
13. Cacciato, M.; Nobile, G.; Scarcella, G.; Scelba, G. Real-time model-based estimation of SOC and SOH for energy storage systems. *IEEE Trans. Power Electron.* **2017**, *32*, 794–803. [[CrossRef](#)]
14. Takagi, T.; Sugeno, M. Fuzzy identification of systems and its applications to modeling and control. *IEEE Trans. Syst. Man Cybern.* **1985**, *SMC-1*, 116–132. [[CrossRef](#)]
15. Lam, H.K.; Leung, F.H.F. LMI-based stability and performance conditions for continuous-time nonlinear systems in Takagi-Sugeno's form. *IEEE Trans. TSMCB* **2007**, *37*, 1396–1406. [[CrossRef](#)]
16. Tanaka, K.; Sugeno, M. Stability analysis and design of fuzzy control systems. *Fuzzy Sets Syst.* **1992**, *45*, 135–156. [[CrossRef](#)]
17. Lian, K.Y.; Liou, J.J.; Huang, C.Y. LMI-based integral fuzzy control of DC-DC converters. *IEEE Trans. Fuzzy Syst.* **2006**, *14*, 71–80. [[CrossRef](#)]
18. Mehran, K.; Giaouris, D.; Zahawi, B. Stability analysis and control of nonlinear phenomena in boost converters using model-based Takagi-Sugeno fuzzy approach. *IEEE Trans. Circuits Syst. I Reg. Pap.* **2010**, *57*, 200–212. [[CrossRef](#)]
19. Chang, Y.C.; Chen, C.H.; Zhu, Z.C.; Huang, Y.W. Speed control of the surface-mounted permanent-magnet synchronous motor based on Takagi-Sugeno fuzzy models. *IEEE Trans. Power Electron.* **2016**, *31*, 6504–6510. [[CrossRef](#)]

